International Journal of Heat and Fluid Flow 30 (2009) 471–480

Contents lists available at ScienceDirect

International Journal of Heat and Fluid Flow

journal homepage: www.elsevier.com/locate/ijhff

Large Eddy Simulation of an evaporating acetone spray

M. Bini, W.P. Jones *

Department of Mechanical Engineering, Imperial College London, Exhibition Road, London SW7 2AZ, UK

ARTICLE INFO

Article history:
Received 30 September 2008
Received in revised form 10 March 2009
Accepted 12 March 2009
Available online 1 May 2009

Keywords:
Large Eddy Simulation
Sprays
Turbulence
Evaporation

ABSTRACT

The LES-Lagrangian particle methodology is applied to the study of vaporizing particle laden flows. A probabilistic description of the liquid phase is adopted and stochastic models for the filtered Lagrangian rates of change of droplet mass and temperature of the spray are presented. The method is applied to an acetone spray which issues into an air co-flow to form an evaporating droplet laden jet. Comparisons of the LES results with measurements demonstrate that the essential features of the flow are reproduced to a good accuracy.

1. Introduction

Aircraft gas turbines are invariably fuelled by kerosene which is introduced into the combustion chamber via a fuel injector. In conventional devices the fuel exits the injector as a thin column or sheet that breaks up to form large droplets or filaments. The initial (primary) breakup is typically a result of a Rayleigh type instability which yields liquid fragments that are of size related to the dimensions of the injector, Lefebvre (1989). These fragments then breakup further (secondary breakup) to form droplets. The distance taken for the droplets to form and their size depends on the injector design but typically they fall within the range 10–100 μm diameter. The velocities of the droplets also depends on injector conditions, droplet size and position. They are dispersed under the influence of the surrounding gas-phase – the continuous phase – evaporate as a result of heat transfer and the gaseous fuel mixes with air whereupon combustion occurs. If the properties of combusting sprays are to be accurately predicted then models of the dispersion and evaporation processes are required. There exists several comprehensive reviews of two-phase flow simulation and modelling techniques (Crowe, 1982; Faeth, 1983b; Crowe et al., 1996; Enwald et al., 1996; Shirolkar et al., 1996; Mashayek and Pandya (2003)), where such models are described. However much of the previous modelling work has been based on Reynolds averaged approaches.

In the present paper Large Eddy Simulation, LES, is applied to a jet laden with liquid droplets of acetone which disperse and evaporate. LES provides a much more detailed description of the dynamics of turbulent flows than does Reynolds average approaches and consequently it should lead to more accurate and reliable results. The configuration considered corresponds to that studied experimentally by Chen et al. (2006) in which properties of both the dispersed and continuous phase are measured far downstream of the injector. At the entrance to the measuring section the spray is dilute and so droplet formation and droplet–droplet interactions are negligible. A Lagrangian formulation of the dispersed phase is combined with an Eulerian description of the continuous phase. A probabilistic approach is adopted for the droplets with the influence of sub-grid fluctuations on dispersion and evaporation being accounted for by means of stochastic models. The results of the computations are compared with measurements.

2. Mathematical formulation

The LES equations can be obtained by applying a spatial filter to the equations of motion. The spatially filtered value of a function $\psi = \psi(\mathbf{x},t)$ is defined as its convolution with a filter function, G, according to:

$$\bar{\psi}(\mathbf{x}) = \int_{\Omega} \psi(\mathbf{y}) G(\mathbf{x}-\mathbf{y}; \Delta(\mathbf{x}))d\mathbf{y} \quad (1)$$

where the integration is carried out over the entire domain, Ω. The filter function, G, has a width Δ which may vary with position. In many problems, including the present case, it is desirable that G is positive definite so that a sub-grid probability density function may be defined. In situations where fluid density variations arise the most straightforward method of accounting for these is through the introduction of density weighted (or Favre) filtering: $\tilde{\psi} = \overline{\rho\psi}/\bar{\rho}$.

* Corresponding author. Tel.: +44 (0)207594 7037.
E-mail address: w.jones@imperial.ac.uk (W.P. Jones).

0142-727X/$ - see front matter © 2009 Elsevier Inc. All rights reserved.
doi:10.1016/j.ijheatfluidflow.2009.03.005

For the properties and limitations of the filtering approach the reader is referred to Germano (1992, 1986) and Piomelli (1999).

Applying density weighted filtering to the equations governing two-phase flow then gives:

$$\frac{\partial \bar{\rho}}{\partial t}+\frac{\partial(\bar{\rho}\tilde{u}_i)}{\partial x_i}=\bar{S}_{mass} \tag{2}$$

$$\frac{\partial(\bar{\rho}\tilde{u}_i)}{\partial t}+\frac{\partial \bar{\rho}\widetilde{u_i u_j}}{\partial x_j}=-\frac{\partial \bar{p}}{\partial x_i}+\frac{\partial \bar{\sigma}_{ij}}{\partial x_j}+\bar{\rho}g_i+\bar{S}_{mom,i} \tag{3}$$

$$\frac{\partial(\bar{\rho}\tilde{Y})}{\partial t}+\frac{\partial(\bar{\rho}\widetilde{Yu_j})}{\partial x_j}=-\frac{\partial \overline{J_j}}{\partial x_j}+\bar{S}_{species} \tag{4}$$

$$\frac{\partial(\bar{\rho}\tilde{e})}{\partial t}+\frac{\partial(\bar{\rho}\widetilde{eu_j})}{\partial x_j}=-\frac{\partial \overline{pu_j}}{\partial x_j}-\frac{\partial \overline{q_j}}{\partial x_j}+\frac{\partial \overline{\sigma_{ij}u_i}}{\partial x_j}+\bar{\rho}g_i\tilde{u}_i+\bar{S}_{energy} \tag{5}$$

As a result of the filtering process the quantities $\bar{\rho}\widetilde{u_i u_j}$, $\bar{\rho}\widetilde{Yu_j}$ and $\bar{\rho}\widetilde{eu_j}$ are unknown and modelling – to account for sub-grid scale, (*sgs*), contributions – is thus required. The filtered source terms can be interpreted as follows: if a particle, p, located at position $\xi^{(p)}$ provides a contribution $S^{(p)}$ to the sources for mass, momentum or energy then the total contribution of the particles within a filtering 'volume' to the source is just the volume average of the individual contributions, viz:

$$\bar{S}(\mathbf{x})=\frac{1}{\Delta^3}\sum_p\int_\Omega S^{(p)}\delta(\xi^{(p)}-\mathbf{y})G(\mathbf{x}-\mathbf{y};\Delta(\mathbf{x}))d\mathbf{y} \tag{6}$$

where the summation is extended over all the particles present in the domain Ω. In writing Eqs. (2)–(5) it has been assumed that the filter width is invariant in space. However, this is not the case in practical applications, where the need for different levels of spatial resolution across the solution domain requires the use of variable grid spacings and this results in a *commutation error*. Providing the mesh spacings are slowly varying, as in the present case, this commutation error can be shown to be almost entirely dissipative in nature and negligible compared with the dissipation provided by the *sgs* model (Wille, 1997).

2.1. Sub-grid models

LES of inert flows have been studied extensively and the simplest model for the sub-grid stress tensor,

$$\tau_{ij}\equiv\bar{\rho}\widetilde{u_i u_j}-\bar{\rho}\tilde{u}_i\tilde{u}_j$$

is the eddy viscosity model of Smagorinsky (1963)

$$\tau^a_{ij}=-2\mu_{sgs}\tilde{S}_{ij}. \tag{7}$$

where

$$\mu_{sgs}=\bar{\rho}(C_s\Delta)^2\|\tilde{S}\|,\quad \tilde{S}_{ij}=\frac{1}{2}\left(\frac{\partial\tilde{u}_j}{\partial x_i}+\frac{\partial\tilde{u}_i}{\partial x_j}\right)\quad\text{and}\quad \|\tilde{S}\|=\sqrt{2\tilde{S}_{ij}\tilde{S}_{ij}}$$

which linearly relates the anisotropic part of the sub-grid stress tensor τ^a_{ij} to the filtered rate of strain tensor $\tilde{S}_{ij}$ via an eddy viscosity coefficient μ_{sgs}. For low speed flows, such as considered here, the isotropic part of the stress can be adsorbed into the definition of the pressure to yield a pseudo-pressure and modelling of this is not then required.

The length scale Δ is related to the filter width that, in LES practice, is invariably assumed proportional to some local measure of the mesh spacing. A commonly used measure is $\Delta=(\Delta_{x_1}\Delta_{x_2}\Delta_{x_3})^{\frac{1}{3}}$ where Δ_{x_1}, Δ_{x_2} and Δ_{x_3} are the physical grid spacings in the three coordinate directions. In the present case, where a variable mesh spacing is employed, the filter width is taken equal to the cube root of the local finite volume cell. The model contains an adjustable parameter C_s, which must be specified. However, as many previous studies have demonstrated and, consistent with the ideas of Kolmogorov, results are found to be relatively insensitive to the value of C_s, providing of course that the turbulence Reynolds numbers are high and the large scale turbulent motions are adequately resolved. In circumstances where this is not the case, for example in transitional flows or in near wall viscous sub-layer regions where adequate mesh resolution is often not possible, various dynamic calibration procedures offer some advantage, e.g. Germano (1992), Piomelli and Liu (1995), and increase the generality of the model. In the present case, however, a single value, $C_s = 0.07$ has been selected. For the sub-grid scalar flux J_k it is usual to adopt a gradient model, see Schmidt and Schumann (1989), of the form:

$$J_k\equiv\bar{\rho}\widetilde{u_k Y}-\bar{\rho}\tilde{u}_k\tilde{Y}=-\frac{\mu_{sgs}}{\sigma_{sgs}}\frac{\partial\tilde{Y}}{\partial x_k}$$

where σ_{sgs} is the sub-grid Schmidt number for which, following Branley and Jones (1999, 2001), a value of 0.7 has been assigned.

A probabilistic description of the spray is adopted with the state of the spray being characterised uniquely in terms of the droplet radius, the droplet velocity, the droplet temperature and number, n. The required joint *pdf* is $\overline{\mathrm{P}}_{spr}(\mathbf{V},\mathrm{R},\Theta,\mathrm{N};\mathbf{x},t)$, where $\{\mathbf{V},\mathrm{R},\Theta,\mathrm{N}\}$ is the 'phase' space for $\{\mathbf{v},\mathrm{r},\theta,\mathrm{n}\}$, which can be obtained, after suitable modelling, from:

$$\frac{\partial\overline{\mathrm{P}}_{spr}}{\partial t}+\nabla_{\mathbf{v}}\cdot\left(\mathbf{a}\overline{\mathrm{P}}_{spr}\right)+\frac{\partial\left(\dot{\mathscr{R}}\overline{\mathrm{P}}_{spr}\right)}{\partial R}+\frac{\partial\left(\dot{\mathscr{T}}\overline{\mathrm{P}}_{spr}\right)}{\partial\Theta}+\frac{\partial\left(\dot{\mathscr{N}}\overline{\mathrm{P}}_{spr}\right)}{\partial N}=0 \tag{8}$$

where $\mathbf{a},\dot{\mathscr{R}},\dot{\mathscr{T}},\dot{\mathscr{N}}$ represent:

$$\mathrm{E}\left(\frac{\mathrm{D}\psi_k}{\mathrm{D}t}\middle|\boldsymbol{\Psi}=\boldsymbol{\Phi}\right)\text{ where }\boldsymbol{\Phi}=\mathbf{v},\mathrm{r},\theta\text{ and n}$$

where $\mathrm{E}\left(\frac{\mathrm{D}\psi_k}{\mathrm{D}t}|\boldsymbol{\Psi}=\boldsymbol{\Phi}\right)$ is the expect value of $\frac{\mathrm{D}\psi_k}{\mathrm{D}t}$ conditioned upon $\boldsymbol{\Psi}=\boldsymbol{\Phi}$ anywhere in the filter volume.

In order to solve the modelled form of Eq. (8) it is first replaced with an equivalent system, Gardiner (2002), of stochastic ordinary differential equations describing the trajectories of stochastic particles in the phase space $\{\mathbf{V},\mathrm{R},\Theta,\mathrm{N}\}$.

The unclosed terms appearing in Eq. (8) are decomposed as follows:

$$\mathrm{E}\left(\frac{\mathrm{D}\psi_k}{\mathrm{D}t}\middle|\boldsymbol{\Psi}=\boldsymbol{\Phi}\right)=f(\psi_k,\tilde{\phi}_{gas};t)+\chi_k \tag{9}$$

where the first term on the *rhs* of Eq. (9) represents a deterministic contribution to the Lagrangian rate of change evaluated in terms of the filtered gas-phase properties $\tilde{\phi}_{gas}$ etc and where χ_k represents the effects of the *sgs* fluctuations on the filtered conditional Lagrangian rates of change for which modelling is required. In the present case two model are required. Firstly a closure approximation is needed for the rate of change of particle velocity – particle acceleration – that is responsible for sub-grid scale particle dispersion. Secondly a model is required for droplet vaporisation in order to determine the rates of change of temperature and size. These are described below.

2.2. Particle acceleration: dispersion

The model for the particle acceleration, $\mathbf{a}$, is directly responsible for particle dispersion in a turbulent flow field. The deterministic part is taken to be equal to the first term of the Maxey and Riley (1983) formulation for the force per particle mass:

$$\mathbf{a}=\frac{\mathrm{D}\mathbf{v}_p}{\mathrm{D}t}=\frac{\tilde{\mathbf{u}}-\mathbf{v}_p}{\tau_p}+\boldsymbol{\chi} \tag{10}$$

where $\mathbf{v}_p$ is the particle velocity, $\tilde{\mathbf{u}}$ is the known filtered gas-phase velocity at the particle position and τ_p is the particle response time:

$$\tau_p^{-1}=\frac{3}{8}\frac{\rho_g}{\rho_f}C_D\frac{|\tilde{\mathbf{u}}-\mathbf{v}_\mathbf{p}|}{r_p} \tag{11}$$

where r_p is the particle radius and C_D is the particle drag coefficient which is determined using the drag law of Yuen-Chen, see Sirignano (1999).

Following Bini and Jones (2007, 2008) a stochastic Markov model is used to represent the influence of unresolved *sgs* velocity fluctuations on particle accelerations and hence dispersion. Thus the acceleration of the *p*th stochastic particle is obtained from:

$$d\mathbf{v}_p = \tau_p^{-1}(\bar{\mathbf{u}} - \mathbf{v}_p)dt + \sqrt{C_0 \frac{k_{sgs}}{\tau_t}} d\mathbf{W} + \mathbf{g}dt \tag{12}$$

where k_{sgs} is the sub-grid kinetic energy of the gas-phase, C_o is a model constant, $d\mathbf{W}$ represents the increment of the Wiener process, $\mathbf{g}$ is the gravitational acceleration vector and τ_t is a time scale which determines the rate of interaction between the particle and gas-phase turbulence. As is shown in Bini and Jones (2007) the model, Eq. (12), through a suitable choice of the time scale τ_t, is capable of reproducing the observed heavy tailed *pdfs* and high levels of probability of extreme acceleration events. A timescale given by:

$$\tau_t = \frac{\tau_p^{2\alpha}}{\left(\frac{\Delta}{\sqrt{k_{sgs}}}\right)^{2\alpha-1}} \tag{13}$$

with $\alpha = 0.8$, was shown to reproduce the high values of kurtosis and *pdfs* observed experimentally. The model is also shown (Bini and Jones, 2008), to be capable of representing accurately particle dispersion in a droplet laden turbulent mixing layer.

2.3. Rate of change for the droplet temperature and size

Miller et al. (1998) reviewed most of the well established vaporisation models, treating both the equilibrium and non-equilibrium vaporisation cases. They demonstrated that various different vaporisation models performed nearly identically for low evaporation rates at gas temperatures lower than the liquid droplet boiling temperature. Only for gas temperatures at and above the liquid boiling point are large deviations to be found between the various formulations. It was noted that, far from critical conditions, there is often a much greater sensitivity of the vaporisation laws to the choice of particular physical constants and liquid properties than to a model change. Following Miller et al. (1998) the temperature and mass rates of change can be written as:

$$\frac{dT^{(p)}}{dt} = \frac{NuCp_g}{3Pr_g Cp_\ell}\left(\frac{T_g - T^{(p)}}{\tau_p}\right) + \frac{h_{fg}}{Cp_\ell}\frac{\dot{m}^{(p)}}{m^{(p)}} \tag{14}$$

$$\dot{m}^{(p)} = \frac{dm^{(p)}}{dt} = -\frac{Sh}{3Sc_g}\left(\frac{m^{(p)}}{\tau_p}\right)H_M \tag{15}$$

where the superscript (p) represents the *p*th particle, T_g is the carrier gas temperature, h_{fg} is the latent heat of evaporation, Cp_g and Cp_ℓ are the gas and liquid specific heats, τ_p is the droplet response time, Pr_g and Sc_g are the gas-phase Prandtl and Schmidt numbers and ρ_g is the density of the gas-phase. *Nu* and *Sh* are the Nusselt and Sherwood numbers modified (Abramzon and Sirignano (1989)) to account, in the presently used convection model, for boundary layer effects.

While different correlations could be adopted, see for instance Lavender and Pei (1967), Birouk and Gokalpb (2006), Faeth (1983a), in the present work the unmodified values of Nusselt and Sherwood number (Nu^*,Sh^*) are evaluated using the model of Ranz and Marshall (1952a,b). This correlation, which is widely recognized to be accurate and is easy to implement, is:

$$Nu^* = 2 + 0.552 \cdot Re_d^{1/2} \cdot Pr_g^{1/3}$$
$$Sh^* = 2 + 0.552 \cdot Re_d^{1/2} \cdot Sc_g^{1/3} \tag{16}$$

where Re_d is the Reynolds number evaluated in terms of the gas properties, the relative velocity and the particle diameter.

The modification proposed in Abramzon and Sirignano (1989) consists of correcting the Nusselt and Sherwood numbers according to:

$$Nu = 2 + \frac{Nu^* - 2}{F_T}$$
$$Sh = 2 + \frac{Sh^* - 2}{F_M} \tag{17}$$

where the correction factors:

$$F_T = (1 + B_T)^{0.7}\frac{ln(1 + B_T)}{B_T}$$
$$F_M = (1 + B_M)^{0.7}\frac{ln(1 + B_M)}{B_M}$$

are evaluated in terms of the energy and mass transfer numbers, B_T and B_M through consideration of a laminar boundary layer developing over an evaporating surface. The two transfer numbers were first introduced by Spalding (1953) and are defined by:

$$B_T = (T_g - T_d)\frac{Cp_{vap}}{h_{fg}} \quad B_M = \frac{Y_s - Y_g}{1 - Y_s} \tag{18}$$

where Cp_{vap} is the liquid vapour specific heat at constant pressure and Y_s is the mass fraction of the vapour at the droplet surface. This latter quantity is determined via an *equilibrium* assumption using the Clausius–Clapeyron equation. H_M, the corresponding convective correction term for mass transfer (Abramzon and Sirignano (1989)) is then obtained from:

$$H_M = ln(1 + B_M)$$

2.4. Stochastic modelling of sub-filter vaporisation

In Bini and Jones (2007) *sgs* particle accelerations – that is unresolved accelerations arising from the interaction between the continuous and dispersed phases – were accounted for by a stochastic formulation based on a multi-dimensional Wiener process. In the context of the rate of change of droplet temperature and mass a similar approach is adopted. The modelled Eqs. (14) and (15) can be viewed as being accurate provided that the complete flow variables are available. In a LES the relative velocity between the droplets and the flow is not completely known and the gas-phase temperature and vapour mass fraction (which also controls the rate of vaporisation) are filtered versions of the complete instantaneous fields. As a consequence if Eqs. (14) and (15) are evaluated solely in terms of filtered values then the effects of sub-filter fluctuations would not be included. It has been previously noted that the temperature rate of change is much less important than the mass vaporisation rate when determining the vaporisation of a single droplet in a non-combusting gas. Consequently in the present work the temperature rate of change is evaluated in terms of the filtered values and attention is focused on *sgs*-modelling of $dm^{(p)}/dt$ which, when treated in a stochastic manner, will also indirectly contribute to stochastic fluctuations in the temperature rate of change.

The method proposed in order to account for unresolved subgrid velocity fluctuations is as follows: the parameter governing convection, *Sh*, is rewritten as the sum of the resolved contribution and a random part so that:

$$dm^{(p)} = -H_M \frac{m^{(p)}}{3\tau_p Sc_g}\left(Sh^{(d)} + Sh^{(st)}\right)dt \tag{19}$$

where $Sh^{(d)}$ is given by the corrected Ranz–Marshall correlation, Eq. (17), evaluated using the LES filtered flow variables and the mixture properties arising in the LES context. $Sh^{(st)}$ accounts for the missing *sgs* turbulence effects, which should vanish as LES approaches DNS and be consistent with the Ranz–Marshall correlation (i.e. capture in a similar fashion unresolved effects). Thus the stochastic contribution to Eq. (19) is represented by:

$$Sh^{(st)}dt = C_V Sc_g^{1/3}\left(\rho_g \frac{k_{sgs}^{1/2} D}{\mu_g}\right)^{1/2} |dW_t|^{1/2}\tau_p^{3/4} \tag{20}$$

where dW_t represents the increment of a Wiener process. The model formulated will add both a random drift and diffusion to the way the droplet mass evolves. C_V is a model constant assigned a value of unity.

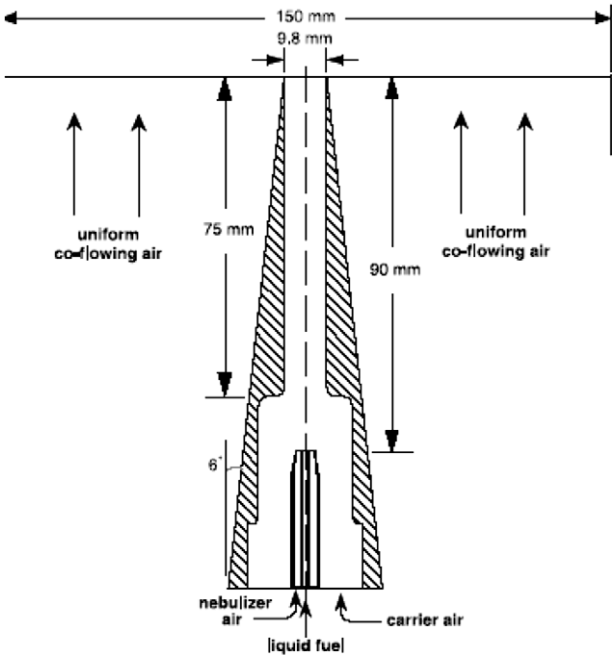

Fig. 1. Detail of the Nozzle and droplet production apparatus used in the experiment (Chen et al., 2006).

3. Configuration

LES is applied to the evaporating spray jet of acetone studied experimentally by Chen et al. (2006). Liquid acetone is injected into a confined air stream which issues, at ambient temperature, into a duct forming a droplet laden jet. The saturated vapour pressure of acetone at 20*C* is ≈0.246 bar, 10 times higher than that of water, so that the droplets evaporate without any pre-heating of the carrier air flow. Fig. 1 shows a schematic diagram of the spray nozzle. The spray is generated by a nebulizer and the droplets then mix with carrier air at ambient temperature which is accelerated through a nozzle of overall length 175 mm. The exit of the nozzle corresponds to the inlet plane of the measuring section and here the droplet distribution is approximately uniform. The resulting droplet laden jet issues into a wind tunnel of cross section 150 mm by 150 mm in which the mean air velocity is 3 m/s and the relative turbulence intensity is less than 2%. The conditions at the nozzle exit are dilute with the ratios of the volumetric flow rate of droplets to that of air being in the range of 0.4×10^{-5}–3.0×10^{-5}. As a consequence droplet–droplet interactions can be safely presumed negligible.

The quantities measured included the averaged inflow velocity of the air together with profiles of the longitudinal and radial rms intensities, average droplet mass flux profiles over the circular section of the jet, mean and rms of droplet velocities divided into size

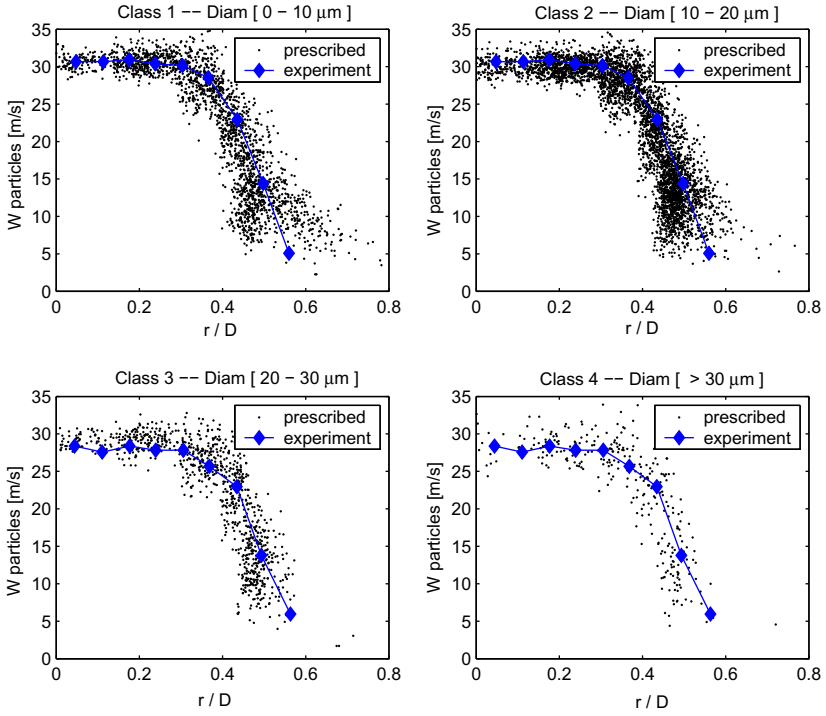

Fig. 2. Longitudinal droplet velocity profiles at $z/D = 1$ for the various diameter classes. Comparison between the mean profiles reported in the experiment and the Stochastic particles prescribed by the sampling procedure for each class during one flow through time.

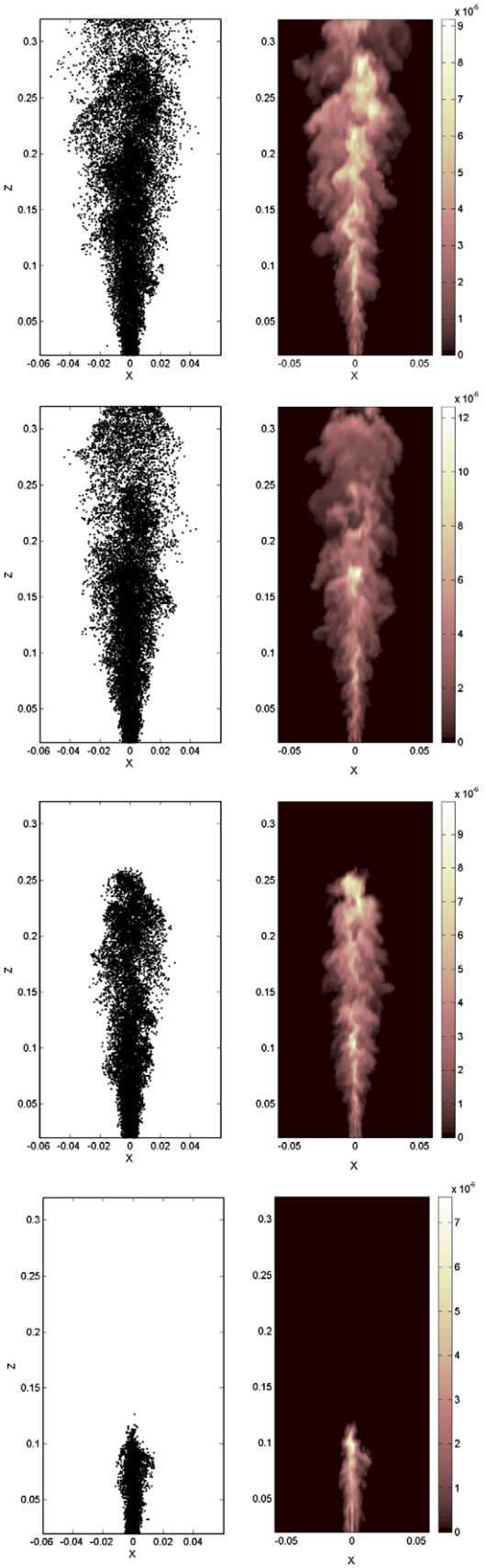

Fig. 3. Instantaneous snapshots of the injection period, case (i): computational droplets (left), vapour mass fraction (right).

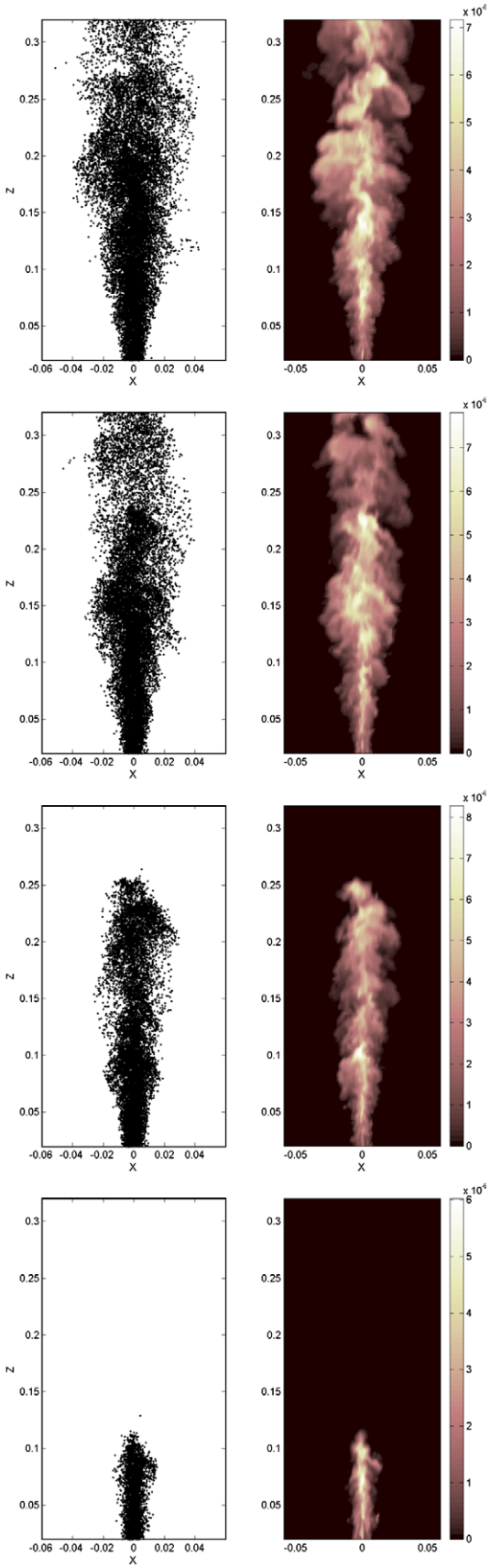

Fig. 4. Instantaneous snapshots of the injection period, case (iii): computational droplets (left), vapour mass fraction (right).

classes and radial profiles of mean droplet diameter. Profiles were measured at various axial locations $0 < \frac{z}{D} \leqslant 25$. Two different jet Reynolds numbers were investigated in the experiments: the present computations consider only the case LFS, Chen et al. (2006), in which the jet has a Reynolds number of 15,800.

The solution domain for the simulations was 150 mm × 150 mm in cross section and extended from the nozzle exit at $z = 0$ to a downstream distance of 500 mm, downstream, i.e. approximately 50 nozzle diameters. The coordinate system used has its origin in the centre of the circular jet with the plane $z = 0$ being coincident with the inflow into the solution domain. For the computations two grids have been used: a grid comprising $59 \times 59 \times 160$ nodes and a larger grid of $85 \times 85 \times 225$ in the x, y and z directions, respectively. Both grids were demonstrated to yield solutions effectively grid independent for the gas field, Bini (2008) and as a consequence the smaller grid was used to obtain the results presented below.

No measurements are available at the inlet plane and inlet boundary conditions have to be estimated. To do this use is made of measured profiles at $z/D = 0.5$: the radial profiles available are acetone vapour mole fraction and mean droplet diameter for droplets in the class sizes $d < 5$ μm, 10 μm $< d <$ 20 μm, 20 μm $< d <$ 30 μm and 30 μm $< d <$ 40 μm together with their corresponding mean and *rms* fluctuating velocities. The inlet profiles are chosen to be consistent with these. However no information concerning the distribution of droplet diameter within the class is available and so little more can be done than to estimate a form for the *pdf* of droplet diameter. To prescribe the *pdf* from which stochastic particles are sampled the jet has been divided in concentric annuli and the *pdf* is presumed to be lognormal with a mean corresponding to that measured at the mean radius of the relevant annulus. During computations the diameter of a stochastic particles is sampled from such a *pdf* and its velocity is assigned using a Gaussian distribution with a mean and standard deviation obtained from the measured profiles for the four classes as a function of radius. This procedure is repeated continuously in time, as the simulation advances, ensuring an average mass flow rate equal to that of the experiment.

The result of the injection procedure is demonstrated in Fig. 2, where the measured average longitudinal droplet inflow velocity is plotted together with that ascribed to the stochastic particles during a mean flow through time. The different number of stochastic particles introduced for every class is a consequence of their prescribed distribution (lognormal). From the figure it is also possible to identify both the different degree of velocity deviation from the mean of the different classes (this was also prescribed and it is maximum for classes 1 and 2 and minimum for class 4), and the fact that the circular inflow has been divided, for discretization purposes, in 5 concentric annulus (this fact appears more distinct for the largest populated class, class 2).

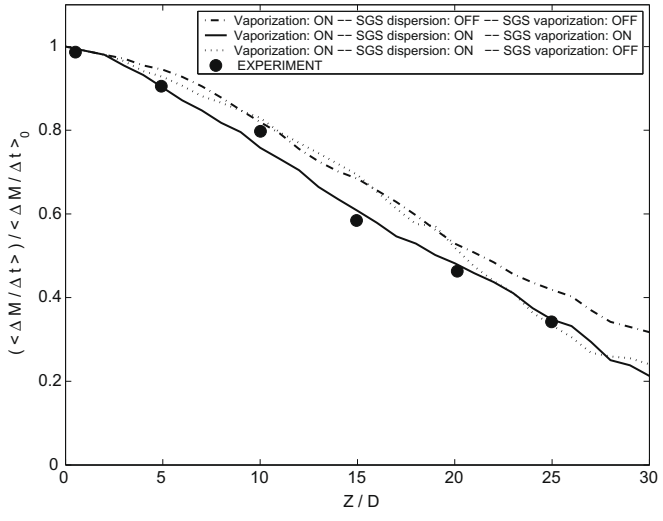

Fig. 5. Downstream flow rate of liquid droplet mass over the whole test section, $\dot{M}(z/D)/\dot{M}(0)$. Case (i) (dash-dotted line), Case (ii) (dotted line), Case (iii) (solid line). Experiments ●.

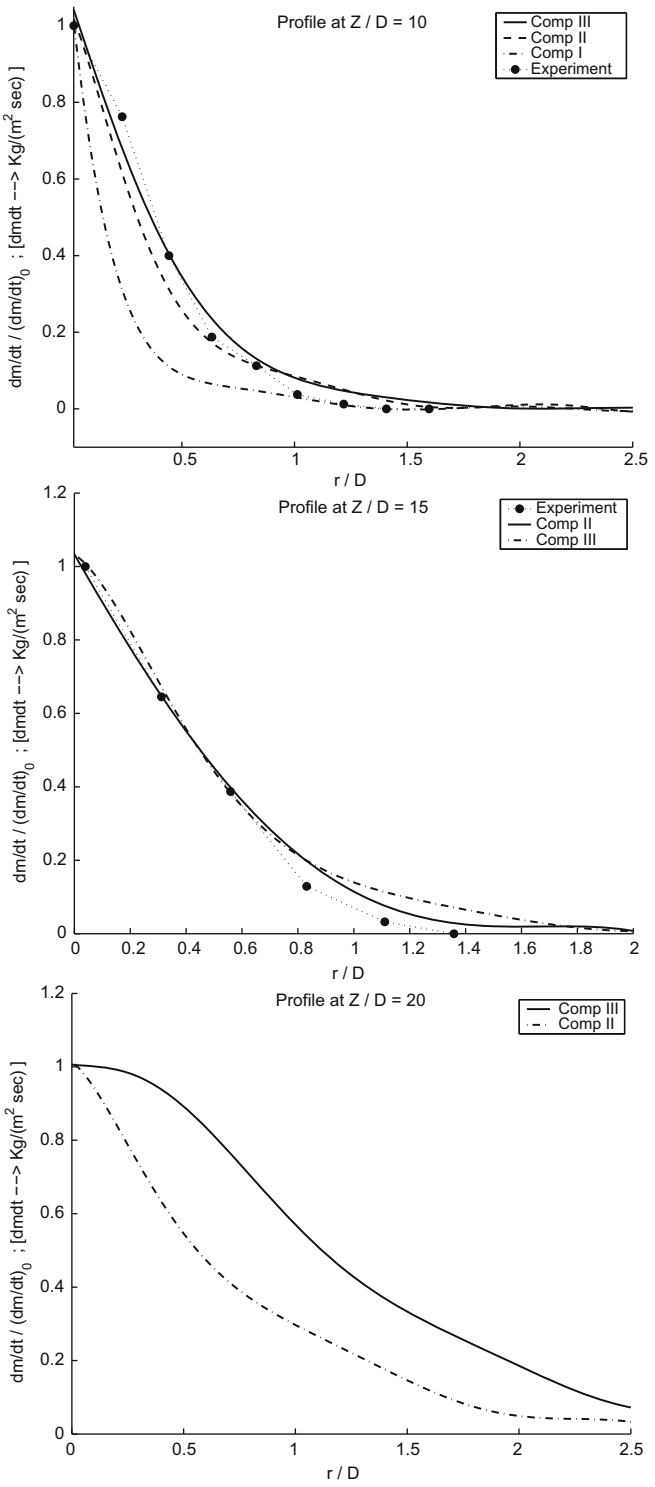

Fig. 6. Radial profiles of liquid droplet mass flux. The value at the centerline of each profile is used as normalization factor.

4. Results

Three simulations were conducted in order to investigate the performance of the evaporation model outlined above. These correspond to the cases where (i) neither the *sgs*-dispersion nor the *sgs*-vaporisation are incorporated, (ii) only the *sgs* dispersion model is employed and (iii) both *sgs*-dispersion and *sgs*-vaporisation are included.

Four instantaneous snapshots of the injection period, i.e. the period of time taken for the spray to occupy the complete length of the computational domain, i.e. 500 mm, are presented for case (i) in Fig. 3 and for case (iii) in Fig. 4. Both the droplet positions and the mass fraction of vapour released by the vaporisation of the droplets are shown. Some clear differences can be observed from an examination of these two sets of instantaneous snapshots. Case (iii) shows relatively higher droplet dispersion (the effect of the *sgs*-acceleration model) and relatively higher vapour mass fractions, i.e. a higher vaporisation rate compared to case (i). In particular the two furthermost downstream snapshots show that the same level of mass fraction obtained in case (iii) at five diameters downstream of the jet entrance occurs about 7–8 diameters downstream for case (i).

The simulated and measured non-dimensional global droplet mass fluxes at different downstream locations, $\dot{M}(z)/\dot{M}(0)$ (where $\dot{M} = [\mathrm{Kg/s}]$) are shown in Fig. 5. The results of the three simulations are shown. The results of case (i) exhibit the lowest vaporisation rate, consistent with the complete omission of *sgs* effects while case (ii) shows a higher downstream rate of mass disappearance though the mass flow rate is over-predicted in the region $5 < z/D < 20$. In contrast the results of case (iii) are in good agreement with the measured values at all downstream location.

Radial profiles of non-dimensional droplet mass fluxes are compared to those measured in Fig. 6. A characteristic feature is that each profile is normalized using the centerline value, an aspect that masks somewhat the differences between the various computations. For example case (i) is characterized by a lower degree of radial dispersion and vaporization and this results in a higher centerline mass flow rate. The effect of this is evident in the profile at $z/D = 10$. The agreement between computed and measured profiles, for the two stations at which data is available, is good for both cases (ii) and (iii). At the furthermost downstream location at $z/D = 20$, however, the mass is found to be distributed in a completely different manner for cases (ii) and (iii). In particular case (ii) has a higher centerline mass flow rate in comparison to case (iii), and the profile exhibits a correspondingly steeper decay. The different shape of the profiles, which is enhanced by the particular normalization procedure adopted, has to be attributed entirely to the sub-filter stochastic evaporation. The likely reason for this is that in case (iii) a higher vapour mass fraction is generated and distributed within the core-jet and that as a consequence mass disappearance is more uniform over the diameter in the far field. In case (ii) the omission of sub-filter evaporation increases the mass of liquid which survives in the core-jet. This suggests that sub-filter acceleration is more influential in droplet vaporization outside the jet whilst sub-filter vaporization is more active in the internal zone of the jet. This is perhaps the opposite of what might have been expected as the driving potential of vaporization B_M, see Eq. (18), is higher the more vapour free is the surrounding gas.

In Fig. 7 the downstream rate of diameter disappearance conditioned upon the initial droplet class is examined for case (*iii*), $\langle D(Z)\text{—}D(0) \in class\ c \rangle$, $c = 1,2,3,4$. The figure displays stochastic particles found in the domain in a specified fraction of time. The higher number of droplets observed in the downstream regions is almost certainly due to the fact that the jet and droplet deceleration is large in the vicinity of the inlet plane; at $z/D = 15$ the stream-wise velocity falls to 30% of the value at the inlet. This coupled together with the clustering effect due to the mushroom like vortices of the shear layer – see also Fig. 4 – is responsible for the increased number of particles downstream of the inlet. Droplets that appertained to class 1 at the inflow plane, ($d \in (0,10]$ μm), are unable to survive for more than about 20 diameters downstream, they completely vaporise. It is also to be noted how the slope of the downstream average diameter change, $\langle dD(Z)/dZ\text{—}D(0) \in class\ c \rangle$, is approximatively comparable

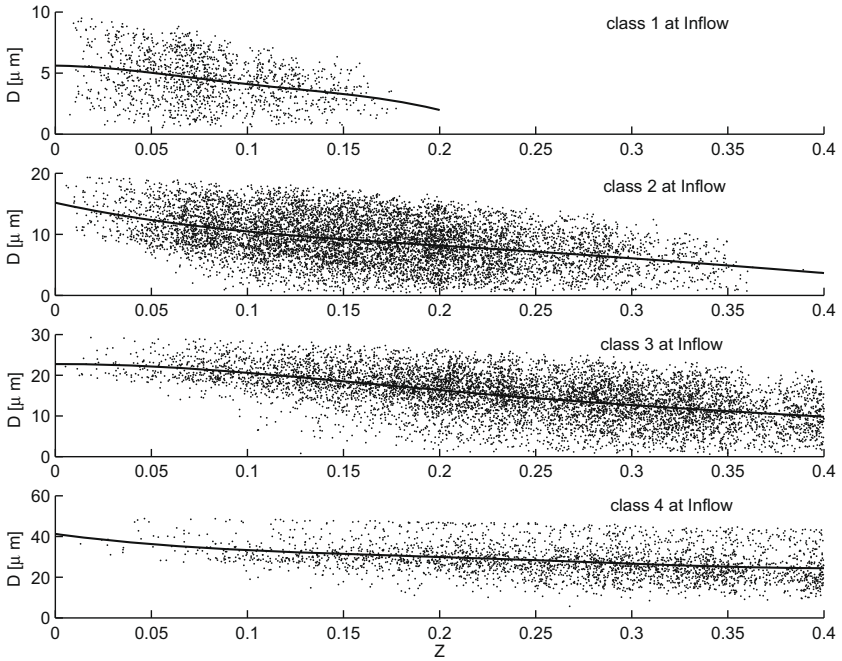

Fig. 7. Rate of downstream droplet diameter disappearance conditioned upon droplet class at inflow, $\langle D(Z)\text{—}D(0) \in class\ c \rangle$. From top to bottom: Stochastic particles for $c = 1,2,3,4$.

for all the classes $c = 1,2,3,4$. The averaged downstream rate of disappearance of an overall class is influenced by many features of the droplet class dynamics, for example by the physical distribution of the class in the domain, by the average velocity of the class, etc. It is well known that the evaporation life time of a single isolated droplet reduces as the diameter is reduced; if the single droplet behaviour applied to the entire class then smaller droplets would vaporise faster than larger droplets. However, in the present situation different classes do not experience the same 'conditions', for example, larger droplets are subject to larger 'slip' velocities (as a result of their larger inertia). The likely explanation for the observed behaviour of $\langle dD/dZ — D \in class\ c \rangle$ is that the similar downstream rates of disappearance between different size classes arise because larger droplets experience more adverse survival conditions than small size droplets. This aspect is discussed further below where it is shown that, on average, large droplets are more likely to be expelled from the jet core than small droplets.

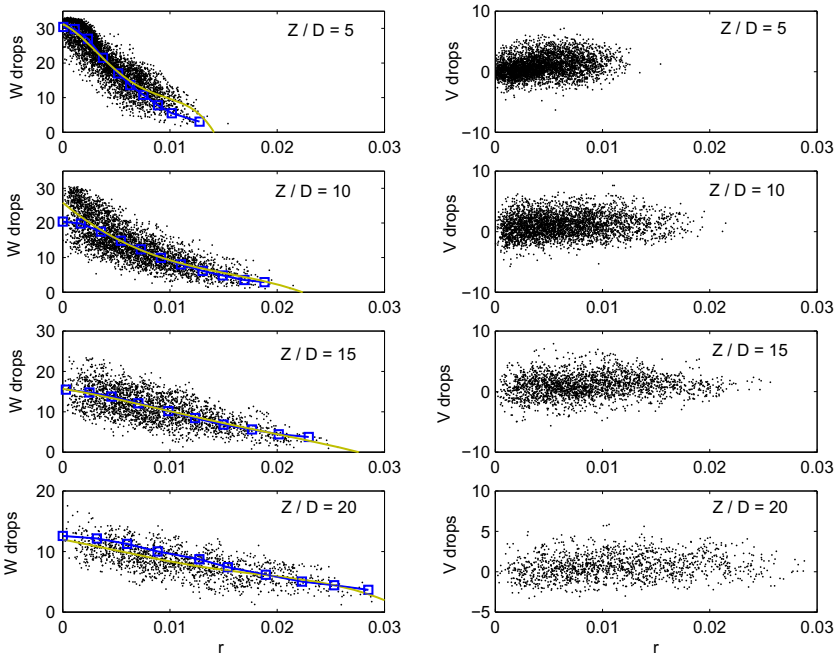

Fig. 8. Radial velocity profiles of droplets appertaining to class 1, $d < 5$ μm. Profiles of longitudinal velocity – left, radial velocity – right. Solid line with squares: experiment; solid line: simulations.

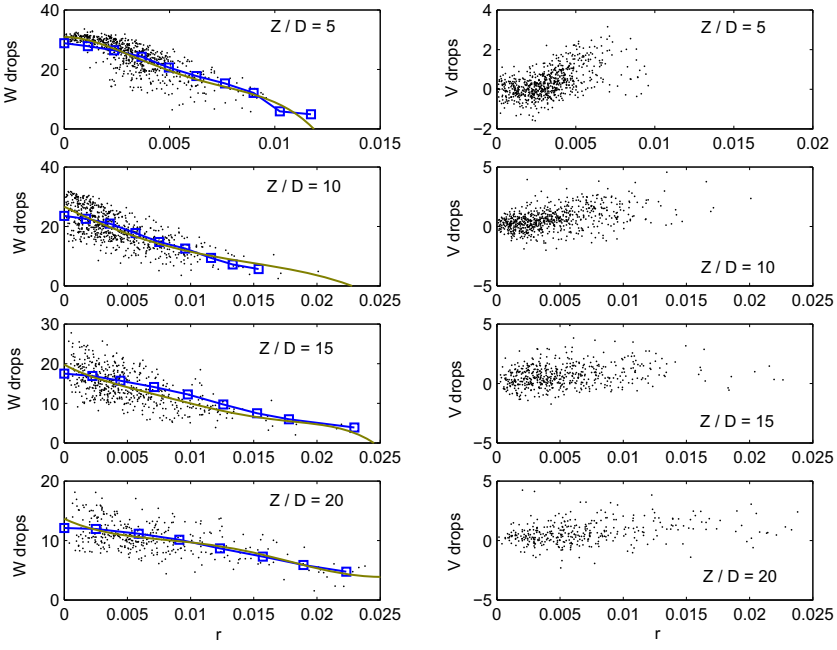

Fig. 9. Radial velocity profiles of droplets appertaining to class 4, 30μm < d < 40μm. Profiles of longitudinal velocity – left, radial velocity – right. Solid line with squares: experiment; solid line: simulations.

Longitudinal and radial droplet velocity profiles at different downstream locations, corresponding to case (iii) and for the two extreme droplet size classes 1 and 4 are compared with the experimental profiles in Figs. 8 and 9. The figures show profiles corresponding to sizes $d < 5$ μm and 30 μm $< d <$ 40 μm, independent of the size at inlet. The diffusive nature of the average droplet transport is remarkably clear as evidenced by the excellent agreement between the simulation and measurement. Accurate prediction of these profiles is a challenge that involves accurate prediction of both dispersion and vaporisation, particularly because droplets undergo a class change: the droplets at the more downstream station used to calculate the velocity profile of class 1 originate from other classes. The profiles, when viewed together with Fig. 7, show that the droplets that appertain to class 1 at the inflow plane, ($d \in (0,10]$ μm), are unable to survive for more than about 20 diameters downstream; they completely vaporise.

A final feature, emphasising once more the effect and importance of the dispersion model, is illustrated in Figs. 10, 11 where class 1 and class 4 velocity profiles are reported, at a downstream location of $Z/D = 5$, for cases (*i*) and (*iii*). Not much difference is re-

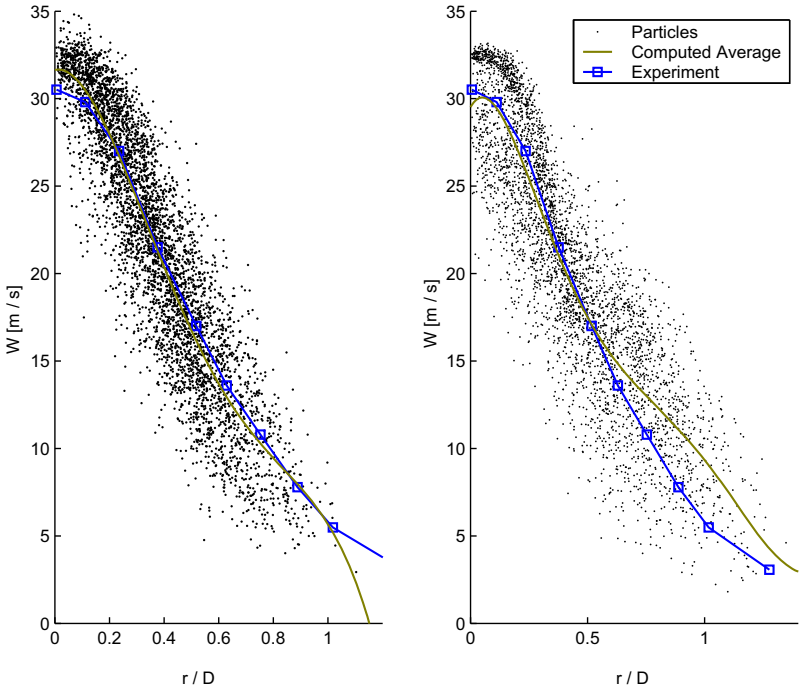

Fig. 10. Radial profile of longitudinal velocity ($Z/D = 5$) for droplets in class 1. Case (i) (left), case (iii) (right).

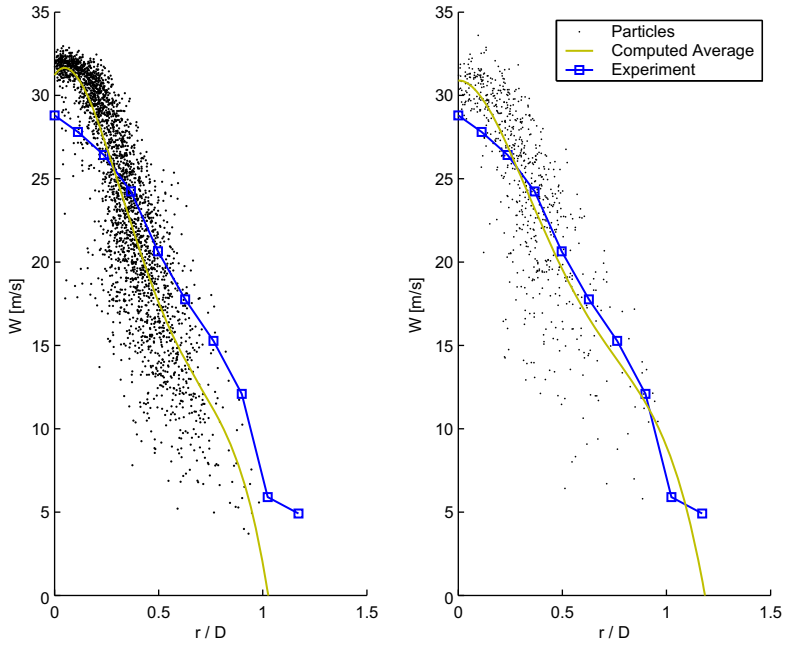

Fig. 11. Radial profile of longitudinal velocity ($Z/D = 5$) for droplets in class 4. Case (i) (left), case (iii) (right).

vealed between the two computations for the profiles of class 1 (the mean profile with *sgs*-acceleration model active is perhaps more diffused than it should be, though this may be attributable to the small number of samples on which the statistics are based at large radial positions). For both cases the velocity in the immediate vicinity of the centreline is overestimated. The reasons for this are unclear though they may arise because of the influence of the estimated inflow boundary conditions on the solutions near the inlet. There are no measurements available for either the dispersed or continuous phase and so the characteristics of both at the inlet are estimated. An important difference between the two cases is evident for class 4. Accurate prediction of the diffusion of large size droplets is particularly important for an accurate prediction of the vaporisation process. In particular neglect of *sgs*-acceleration leads to an unacceptably low lateral spread of droplets, emphasising again the importance of *sgs* effects.

5. Conclusions

The paper has presented deterministic and stochastic closures for the problem of droplet vaporisation within the framework of LES *pdf* methods for particle laden flows using the formalism of generalized stochastic differential equations. The approach is then applied, as a demonstration, to the study of a vaporizing spray of acetone for which detailed measurements are available. The analyses have been tailored to emphasize the importance of sub-filter models. In particular neglect of both *sgs*-acceleration and *sgs*-vaporisation results in very poor predictions. The use of an appropriate sub-filter acceleration model enables a satisfactory representation of the vaporisation rates only in the far field of the jet and the predicted mass disappearance rate in the midfield of the jet improves when stochastic effects are accounted for in the droplet mass rate of change.

Various forms of evidence have been provided to corroborate the complimentary nature of the effects introduced by the two sub-filter models. All of the evidence seems to point to the fact that sub-filter acceleration in addition to being crucial for providing an accurate radial diffusion of large diameter droplets, is also responsible for larger instantaneous droplet acceleration which by itself drives an enhanced convective vaporisation. On the other hand, sub-filter mass evaporation seems to be effective in providing increased mass vaporisation rates in the inner zone of the jet, where the average slip velocity between the phases is likely to be smaller and where, as demonstrated, preferential concentration of small diameter particles takes place. A different state space path of dispersion and vaporisation for droplet of various classes of diameters has been suggested as a possible explanation for this complimentary effect between sub-filter models.

Acknowledgement

The financial support of the European Union under INTELLECT D.M., contract F-AST3-CT-2003-502961, is gratefully acknowledged.

References

Abramzon, B., Sirignano, W.A., 1989. Droplet vaporization models for spray combustion calculations. Int. J. Heat Mass Transfer 32, 1605–1618.
Bini, M., 2008. Large Eddy Simulation of Particle and Droplet Laden Flows with Stochastic Modelling of Sub-filter Scales. Ph.D. Thesis, Imperial College, University of London, London, UK.
Bini, M., Jones, W.P., 2007. Particle acceleration in turbulent flows: a class of nonlinear stochastic models for intermittency and heavy tailed pdfs. Phys. Fluids 19 (3), 035104.
Bini, M., Jones, W.P., 2008. Large eddy simulation of particle laden turbulent flows. J. Fluid Mech. 614, 207–252.
Birouk, M., Gokalpb, I., 2006. Current status of droplet evaporation in turbulent flows. Prog. Energy Combust. Sci. 32, 408–423.
Branley, N., Jones, W.P., 1999. Large eddy simulation of a turbulent non-premixed swirling flame. In: Lawrence, D., Rodi, W. (Eds.), Engineering Turbulence Modelling and Measurements, vol. 4. Elsevier, Amsterdam, Corsica, France, pp. 861–870.
Branley, N., Jones, W.P., 2001. Large eddy simulation of a turbulent non-premixed. Combust. Flame 127, 1914–1934.
Chen, Y.C., Starner, S.H., Masri, A.R., 2006. A detailed experimental investigation of well-defined, turbulent evaporating spray jets of acetone. Int. J. Multiphase Flows 32, 389–412.
Crowe, C.T., 1982. Review: numerical models for dilute gas-particle flows. J. Fluids Eng. 104, 297–303.
Crowe, C.T., Troutt, T.R., Chung, J.N., 1996. Numerical models for two-phase turbulent flows. Annu. Rev. Fluid Mech. 28, 11–43.
Enwald, H., Peirano, E., Almstedt, A.E., 1996. Eulerian two-phase flow theory applied to fluidization. Int. J. Multiphase Flow 22.
Faeth, G., 1983a. Evaporation and combustion of sprays. Prog. Energy Combust. Sci. 9, 1–76.
Faeth, G.M., 1983b. Evaporation and combustion of sprays. Prog. Energy Combust. Sci. 9, 1–76.
Gardiner, C.W., 2002. Handbook of Stochastic Methods. Springer.
Germano, M., 1986. Differential filters for the large eddy simulation of turbulent flows. Phys. Fluids 29, 1755–1757.
Germano, M., 1992. Turbulence:the filtering approach. J. Fluid Mech. 238, 325–336.
Lavender, W.J., Pei, D.C.T., 1967. The effect of fluid turbulence on the rate of heat transfer from spheres. Int. J. Heat Mass Transfer 10, 529–539.
Lefebvre, A.H., 1989. Atomization and Sprays. Taylor and Francis.
Mashayek, F., Pandya, R.V.R., 2003. Analytical description of particle/droplet-laden turbulent flows. Prog. Energy Combust. Sci. 29, 329–378.
Maxey, M., Riley, J.J., 1983. Equation of motion for a small rigid sphere in a nonuniform flow. Phys. Fluids 26, 883–889.
Miller, R.S., Harstad, K., Bellan, J., 1998. Evaluation of equilibrium and non-equilibrium evaporation models for many-droplet gas–liquid flow simulations. Int. J. Multiphase Flow 24, 1025–1055.
Piomelli, U., 1999. Large eddy simulation: achievements and challanges. Prog. Aerosp. Sci. 35, 335–362.
Piomelli, U., Liu, J., 1995. Large Eddy Simulation of rotating channel flows using a localized dynamic model. Phys. Fluids 7 (4), 839–848.
Ranz, W.E., Marshall, W.R., 1952a. Evaporation from drops, part I. Chem. Eng. Prog. 48, 141–146.
Ranz, W.E., Marshall, W.R., 1952b. Evaporation from drops, part II. Chem. Eng. Prog. 48, 173–180.
Schmidt, H., Schumann, U., 1989. Coherent structure of the convective boundary layer derived from large eddy simulation. J. Fluid Mech. 200, 511–562.
Shirolkar, J.S., Coimbra, C.F.M., McQuay, M.Q., 1996. Fundamental aspects of modelling turbulent particle dispersion in dilute flows. Prog. Energy Combust. Sci. 22, 363–399.
Sirignano, W.A., 1999. Fluid Dynamics and Transport of Droplet and Sprays. Cambridge University Press.
Smagorinsky, J., 1963. General circulation experiments with the primitive equations I. The basic experiment. Mon. Weather Rev. 91, 99–164.
Spalding, D.B., 1953. The combustion of liquid fuels. Proc. Combust. Inst. 4, 847–864.
Wille, M., 1997. Large Eddy Simulation of a Plane Jet in a Cross Flow. Ph.D. Thesis, Imperial College, University of London, London, UK.